RSC Advances

ROYAL SOCIETY OF CHEMISTRY

www.rsc.org/advances

TOC figure

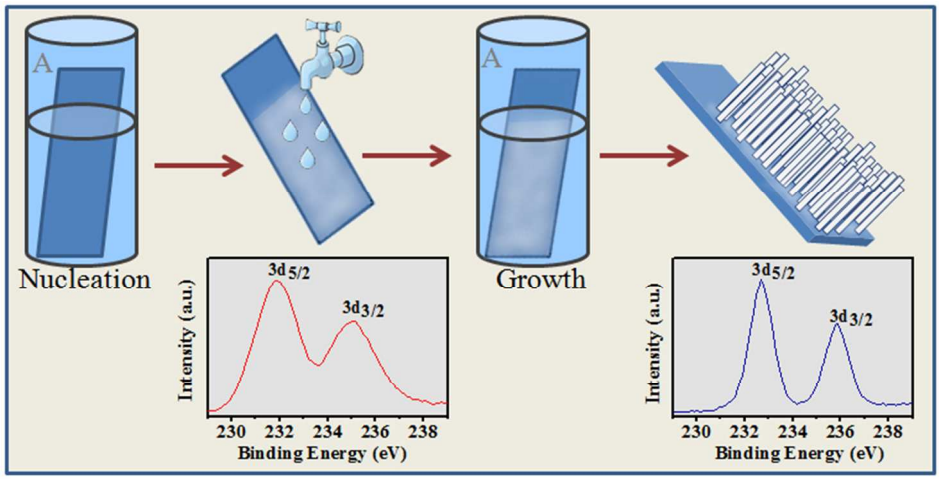

h-MoO_3 nano rods are deposited on FTO substrate by two step chemical bath deposition method.

First stage of the deposition is the nucleation step followed by growth at second stage.

Cite this: DOI: 10.1039/c0xx00000x

www.rsc.org/xxxxxx

ARTICLE TYPE

Two Stage Chemical Bath Deposition of MoO_3 Nanorod Films

Arpan Dhara,[a] Gary Hodes[b] and Shaibal K Sarkar[*,a]

Received (in XXX, XXX) Xth XXXXXXXXX 20XX, Accepted Xth XXXXXXXXX 20XX
DOI: 10.1039/b000000x

Thin films of hexagonal MoO_3 nanorods are deposited by chemical bath deposition from a highly acidic aqueous solution containing ammonium heptamolybdate at 85^0C. We present a unique *two-stage* deposition process that results in uniform film formation even from a highly depleted solution. Growth occurs during the second stage *only* if the substrate removed from the first stage solution is first rinsed with water. Mechanistically, the proposed process is a combination of formation of nucleation sites at the *first stage,* removal or modification of a passivation layer on the nucleation sites by the rinse and chemical heterogeneity-induced growth at the *second stage*. Variations in either of these two deposition stages lead to control over rod dimensions and film texture. An FTIR study confirms the presence of amine and hydroxyl group tightly bound in the crystals. Furthermore, *h*-MoO_3 nanorod films showed good photocatalytic activity towards degradation of methylene blue (MB) under visible light.

1. Introduction

Transition metal oxides and sulfides with layered structures offer interesting applications in various fields ranging from electronics to mechanical lubrication.[1,2,3,4] MoO_3in particular is suitable for a wide range of applications in electronics,[2,5,6] photovoltaic energy conversion[7,8] and electrochemical storage[9,10] applications. The possibility of ion intercalation in layered structures of MoO_3 make it highly pertinent in solid-state Li-ion batteries.[11,12,13] The high work function and low-lying conduction band of MoO_3 is responsible for its ability to facilitate hole removal in organic photovoltaics.[14,15] Apart from its bulk material properties, its nanostructured forms provide an added parameter of high surface to volume ratio that results in higher catalytic,[16,17,18,19] sensing[20] and charge collection[21] efficiencies.

Several studies have described the synthesis of MoO_3 nanostructures of various shapes and sizes. Orthorhombic α-MoO_3,which is the thermodynamically most stable phase, has a unique layered atomic structure, but various other phases are found in the literature.[22,23,24] Most of the reported syntheses involve high temperatures involving mostly gas phase synthesis in high vacuum. Vacuum arc synthesis is one among the many.[25] Bakeret al. described a solution phase synthesis of a high pressure phase of MoO_3.[26] In other studies a mixed phase of α-MoO_3 andβ-MoO_3 (monoclinic) was obtained.[22,23] A popular way to deposit films of MoO_3 is through post-deposition thermal annealing of evaporated Mo metal films.[27] Deposition of MoO3 nanorods or other nano structures were reported but all are high energy process.[28,29,30]

Decomposition of ammonium heptamolybdate (HMA) to form thermodynamically stable α-MoO_3 by a hydrothermal method is well documented. The reaction mechanism in solution can be written as follows:[31]

$$(NH_4)_6Mo_7O_{24}.4H_2O \xrightarrow{\Delta} MoO_3 + 6NH_3 + 7H_2O \quad \ldots\ldots (1)$$

Control over the morphology and particle size can be further obtained by the addition of additives that can complex with the Mo^{6+}. Song et al. reported a simple precipitation method to produce bulk precipitation of hexagonal-MoO_3(h-MoO_3) nanorod structures by acidifying HMA.[32] The isopolymolybdate ions ($Mo_7O_{24}^{6-}$) in the solution were converted to MoO_3 in the presence of excess H^+ ions. The reaction mechanism can be written as

$$Mo_7O_{24} + 6H^+ = 7MoO_3 + 3H_2O \quad \ldots\ldots (2)$$

This opens a new arena to prepare and study the properties of meta-stable *h*-MoO_3 that can be expected to behave differently than the thermodynamically-stable α-MoO_3 phase. Precipitation of *h*-MoO_3 by acidification of HMA was demonstrated in 1987 by Kumagai et al.[33] However it is difficult to distinguish it from its other cation-stabilized form, $MoO_3.nNH_3.mH_2O$[22,34] due to the similarities in the XRD patterns. Apart from the simple precipitation techniques, *h*-MoO_3 was also synthesized through hydrothermal[22,35] and vapor deposition[36] routes. Solution deposition of MoO_3 thin films was much less studied than precipitates. High purity *h*-MoO_3films with good crystallinity were deposited by Deki et al. from a bath containing molybdic acid dissolved in a mixture of HF and boric acid.[37]

In this paper we describe conditions to obtain films of *h*-MoO_3 by acidification of HMA. In this precipitation, no film formation occurred under most conditions and, where it did form, the film quality (coverage) was poor. Based on these results, we developed a unique *two-stage* deposition of good quality, oriented *h*-MoO_3nanorod films by CBD. In the *first stage,* only nucleation occurred on the fluorine-doped tin oxide (FTO)-coated glass substrate, followed by film growth during the *second stage*.

Control over the rod length, diameter and orientation was achieved by controlling the deposition conditions.

2. Experimental

MoO_3 films were deposited from a highly acidic bath containing 0.1-0.05 M of HMA and 5.2 M of HNO_3 in a thermostatically-controlled water bath at 85^0C for 1hr. The deposition solution was placed in an airtight glass vial with the FTO-coated glass substrate placed facing down at a roughly 45^0 angle to the bottom of the vial to avoid accumulation of bulk precipitate on the substrate surface. After deposition, the surface was rinsed thoroughly with DI water before drying with N_2 gas.

For two-stage deposition, 5 ml of 2 M HNO_3 was mixed with 10 ml HMA (concentration varied from 0.1- 0.01 M) solution with continuous stirring. About 10 ml of that solution transferred to a vial and kept into a water bath at 85^0C. Then the FTO substrates were placed into the solution as described earlier for another half an hour. This step is considered as nucleation step. After that, substrates were taken out from the solution and ringed thoroughly with distilled water followed by the growth step where the substrates were again put into the same solution for another half an hour. After deposition, films were washed with distilled water and dried.

Photocatalytic degradation study of methylene blue (MB) dye using *h*-MoO_3 nanorods films were performed in a quartz vessel containing 25 ml dye solution (10 mg/L). Two thin films of h-MoO_3 with active area 2.5x1 cm^2 each were dipped into the dye solution and a tungsten halogen light of 300 W was used as a light source. UV-VIS spectroscopy of the solution as a function of the irradiation time was performed separately.

X-Ray diffraction measurements were performed in theθ-2θ configuration, using a Phillips X'Part diffractometer equipped with a Cu anode operating at 40 kV and 30 mA, emitting a wavelength of 1.54 Å.

Scanning Electron Microscope (SEM) images were taken with a JEOL FESEM using a secondary electron detector. For Transmission Electron Microscopy (TEM), films were scraped from the substrate with a blade and dispersed in water, then put on a grid and dried naturally. TEM imaging was carried out with a JEOL 2100F transmission electron microscope operating at 200kV.

Fourier Transform Infra Red (FTIR) spectroscopy measurements were performed with a Bruker Vertex 70 in transmission mode. Samples were scraped from the film, heated where needed, and mixed well with KBr powder to form pellets.

Absorbance measurements were done with a PerkinElmer Lambda 35 UV-VIS spectrophotometer in absorption mode.

3. Results and discussions

Under highly acidic condition, heating of HMA results in precipitation of MoO_3. In this process, isopolymolybdate ions ($Mo_7O_{24}^{6-}$) in the solution are converted to MoO_3 upon heating at 85^oC (as shown in eq. 2). X-ray diffraction and SEM imaging confirmed the hexagonal crystallographic nature of the powdery precipitate. Film formation was found only on the FTO surface: No film formation was observed on the glass container surface, activated glass (HNO_3 or $KMnO_4$ treated) or any metal substrates tried by us (stainless steel or Au). However we did find film growth occurred also on TiO_2.We did not devote much effort to trying to understand what was special about the FTO and TiO_2. We do note that, since the solution was highly acidic, all substrates are expected to be positively charged and therefore the reason is unlikely to be due mainly to electrostatic forces. All references to films in this paper refer to films on FTO.

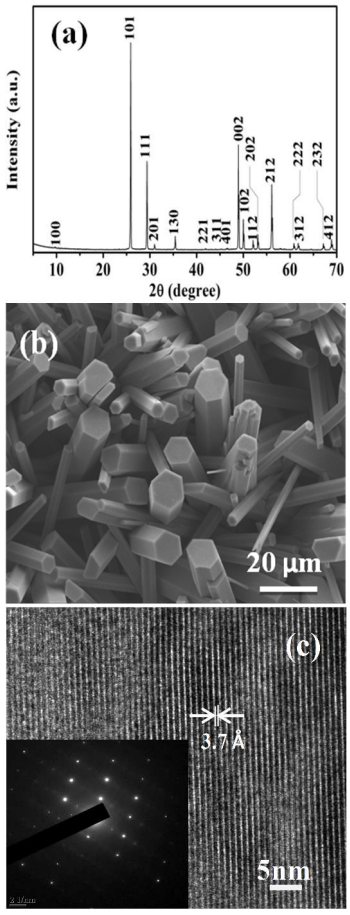

Fig. 1: (a) XRD pattern of the as-deposited films obtained from 0.1M HMA and 5.2M HNO3in the Bragg-Brentano configuration. (b) SEM micrograph revealing hexagonal rod-like morphology of the deposit. (c) TEM image and the SAED pattern showing mono crystallinity of the individual rods

An XRD pattern of a representative as-deposited film is shown in figure 1a. All the peaks can be indexed to the hexagonal phase of MoO_3. Crystallographic analysis of the pattern reveals a = b = 10.5756Å and c = 3.7209 Å which matches with the Rietveld fitting value done by Pan et al.[38] as well as with other literature values.[34,37] An SEM image of the same film is shown in figure 1b. A rod-like morphology with rod diameter ranging from 2-10 µm and with flat hexagonal top surfaces is clearly seen. A TEM image of a single rod is shown in figure 1c together with selected

Cite this: DOI: 10.1039/c0xx00000x

www.rsc.org/xxxxxx

ARTICLE TYPE

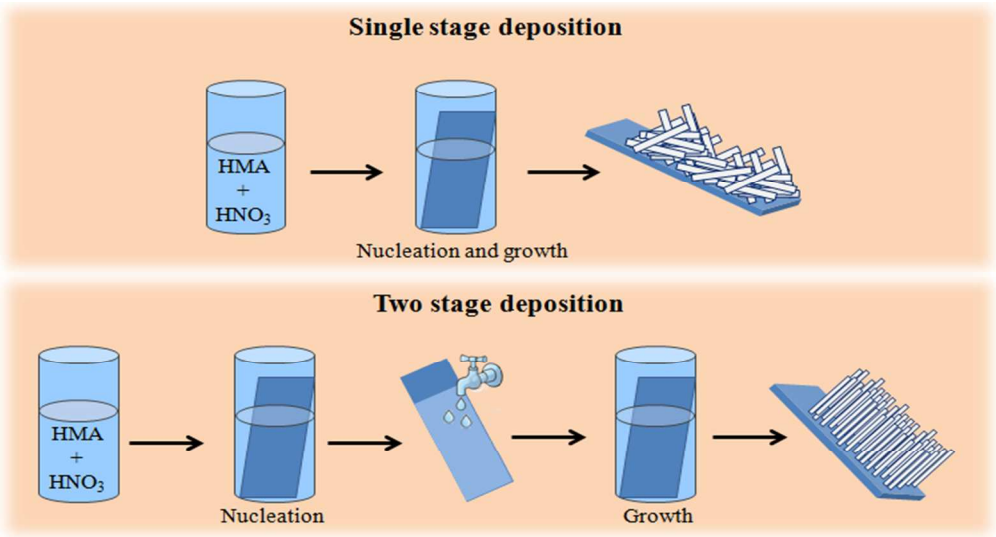

Fig. 2: Schematic representation of single stage and double stage deposition process of h-MoO_3 nanorod films

point-like ED pattern, reveals the single crystalline nature of the individual rods.

Semi-quantitative XPS elemental analysis of the as deposited films (fig. 3a) shows Mo $3d_{5/2}$ and $3d_{3/2}$ peaks at 232.686 eV and 235.847 eV, agreeing with that reported previously for MoO_3.[32,39] However, a considerable amount of nitrogen at 398.6 eV was observed which is chemically different from the nitrogen in metal nitrides. To understand the chemical nature of the nitrogen in the deposit, we performed FTIR transmission measurements on powder scraped from the substrates. As shown in figure3b, –NH bending and stretching peaks were clearly observed at ca. 1440 cm^{-1} and 3228 cm^{-1} respectively.[34,40]Also absorbance from –OH vibrations was found at 1400, 1610 and 3500 cm^{-1}. The peak at 1600 cm^{-1} corresponds to the deformation of free water molecule and that at 1410 is probably the MoO–H bending vibration.[34] To understand the nature of the –OH and –NH peaks, samples were annealed at 200^0C. After this annealing, the –OH peak intensity did not change whereas the –NH peak intensity decreased by ca.

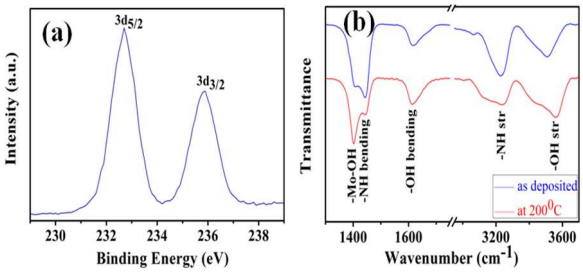

Fig.3: (a) XPS Mo peaks obtained from an as-deposited film (b) FTIR transmission spectra showing N-H and O-H stretching and bending vibrations of as-deposited and air-annealed (at 200 ºC) samples.

50%. The lack of change of the water/OH peaks on annealing suggests that these species are inside the crystals rather than predominantly on the surface, where they (at least the water) would be expected to be strongly reduced in concentration on annealing. The N most likely comes from NH_4^+ that is mainly also inside the crystal – either occluded or as $MoO_3.nNH_3.mH_2O$.

Reducing the relative HMA concentration from 0.1M to 0.05 M, while keeping the HNO_3 concentration unaltered (5.2 M), resulted in a decrease of both the rod diameter and the surface coverage as shown in figure 4 (a-c).While the rod formation can be attributed to the higher reactivity of the (101) surface, the low material concentration resulted in poor surface coverage. Low ionic concentration favors lower nucleation density on the substrate. Similar behavior was observed during ZnO growth in the presence of relatively low concentrations of Zn^{+2}.[41]

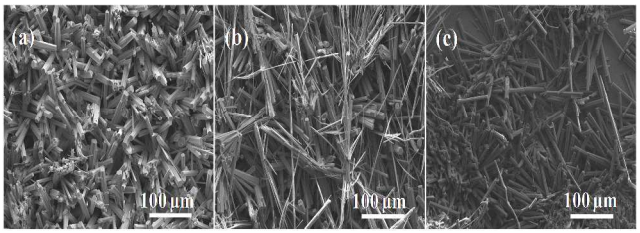

Fig. 4: Scanning Electron Micrograph of the films obtained with (a) 0.1M, (b) 0.065 M and (c) 0.05 M HMA concentration. The HNO_3 concentration was constant at 5.2 M.

The film formation largely depends on the acid concentration in the deposition solution. No visible deposition occurs if the acid concentration is reduced below 5.2 M, other deposition parameters remaining unaltered, although bulk precipitation occurs in the solution even at much lower acid concentration (>0.05 M).The rate of this precipitation depends on the net acid

concentration in the solution. After addition of the acid to the HMA solution at 85°C, the transparent solution slowly turns increasingly turbid, then gradually transparent again as the suspension precipitates. To exemplify the dependence of these processes on HNO_3 concentration, for 5.2 M HNO_3 with 0.1 M HMA, it takes one min for the solution to become cloudy and another10 min to clear, indicating the completion of bulk precipitation. Reducing the acid concentration, it requires more time for the solution to become turbid and the turbidity persists for a longer time. Thus reduction in acid concentration in the deposition solution lowers the reaction rate. The above-described behavior also clearly indicates that homogeneous nucleation occurs in the bulk of the solution, resulting in a suspension that finally precipitates. In parallel with homogeneous nucleation and precipitation, nucleation and growth obviously also occurs on the FTO substrate (but not on most other substrates we tried).

However, when a substrate that was removed from the reaction solution after 30 min and showed no visible deposit, was rinsed with DI water and then again immersed in the same (or a fresh) solution, a highly uniform film was deposited. In this paper, we identify such a film as a *second stage* deposition, while the initial 30 min treatment is identified as a *first stage* deposition. The bulk precipitation that occurred during the first stage of the two-stage reaction considerably lowered the molybdenum concentration in the solution. Before describing these deposits, since it is clear that, although no visible deposit formed after the first stage, there is some effect of this first stage treatment, most likely nucleation of some species, we investigated more closely this first stage. We studied the substrate after 30 min in the (5.2 M) deposition solution.

While FESEM images revealed no distinct particles that might be attributed to nuclei, XPS clearly indicated the presence of Mo^{+6} species on the substrate (Figure 5). The ratio of surface Mo^{+6} to Sn^{+4} (from the FTO substrate) after the first stage was 1:4.25. Assuming the Mo is in the form of discrete nuclei of a Mo-O material (the most likely expected scenario), this would represent a moderately dense coverage of nuclei with comparable diameter and spacing between the nuclei. Taking into account the relatively close atomic numbers of Mo and Sn, and hence correspondingly low contrast expected, nuclei smaller than ca, 10 nm might not be seen in the FESEM. Another, less likely but still possible scenario is that the substrate is covered with a continuous layer, likely to be either amorphous or an adsorbed monolayer. The 1:4.25 Mo:Sn ratio measured could then be roughly estimated to correspond to two monolayers of a Mo-O species. The peaks in Figure 5 are shifted to lower binding energy by ca. 0.6 eV in comparison to the reported Mo $3d_{5/2}$ and $3d_{3/2}$ peaks of MoO_3 (in Figure 3a). This indicates a different chemical environment of the Mo in comparison to the normal MoO_3 lattice. The same XPS peaks of Mo(V), measured in non-stoichiometric amorphous MoO_3 have been measured to be ca. 1 V lower in binding energy compared to the Mo(VI) in stoichiometric films.[42] stage deposition from a solution that contained 0.65 M $HNO_3$and HMA of varying concentrations (0.1, 0.05, 0.025 and 0.01 M, a-d respectively).With reducing HMA concentration in the solution, an increase in the rod diameter and in the film texture was evident. Increase in HMA concentration results in faster bulk precipitation, and it is probable that the actual concentration of soluble Mo species is higher at lower initial HMA concentration and that the concentration falls due to bulk precipitation much more slowly, thus allowing time for more growth. This is supported by the observed effect of aging of the second stage deposition solution.

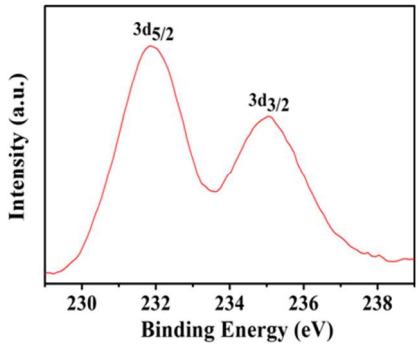

Fig. 5: Mo 3d XPS spectrum after the 1st stage of the two step deposition

The chemical bath deposition process consists of two interlinked steps: nucleation and growth. Often these two processes occur simultaneously, resulting in a large particle size distribution in the film. Separating the nucleation and growth stages leads to a narrower size distribution with better control over the film morphology, as demonstrated previously for ZnO nanorod films.[43] Yang et al showed aligned ZnO nanorod arrays on ZnO nanoparticle-coated Si substrates.[44] A pre-nucleated substrate introduces the heterogeneity that assists the growth. The diameter of the rods was primarily determined by the grain size of the ZnO nanoparticles on the seeded substrate. This was also the case where heterogeneous seeding was used, i.e. the seed layer was not ZnO but a hydrated Mn oxide.[45]

Figure 6 shows SEM images of films obtained after a second

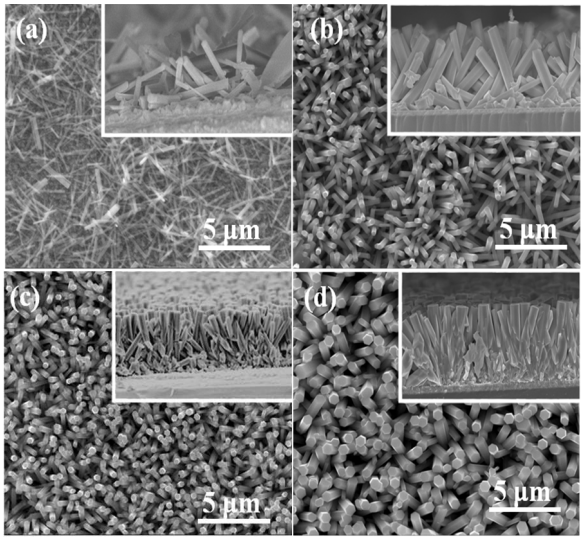

Fig. 6: SEM images of the as-deposited films obtained from (a) 0.1 M, (b) 0.065M (c) 0.025 M and (d) 0.01 M of HMA.

Since homogeneous precipitation gradually occurs in the second stage solution, the reactant concentrations gradually decrease with time. Therefore we expect similar behavior from a fresh low-concentration solution and an aged solution with the same eventual concentration as the fresh low-concentration one.

Figure 7 compares films deposited from a second stage fresh solution (0.025 M HMA and 0.65 M HNO_3) and the same solution, aged for 30 min. We found that the second stage deposition happens also when the concentration of both HMA and HNO_3 was reduced by 50 times; a continuous increase in rod diameter was obtained with reduction in concentration.

Yet further control of the rod diameter can be obtained by controlling the nucleation at the first stage. Figure 8 shows films prepared from a first stage deposition solution containing 0.025M of HMA and 0.65 M HNO_3. The substrates were taken out from the deposition solution after 2, 5,10,20,30 and 45 min. At the *second stage* of the deposition these *pre-treated* substrates were re-immersed in the same aged solution kept at 85^0C for 30 min. The shorter the time in the first stage bath, the greater is the width of the rods. This can be explained in general by lower nucleation density on the substrate resulting in larger rods since the same amount of available reactant is divided by a smaller number of nuclei. Figure 9 shows histogram of rod diameters obtained from different films. If nucleation is by a continuous layer of a Mo species, this explanation could still hold assuming that the layer formation occurs slowly.

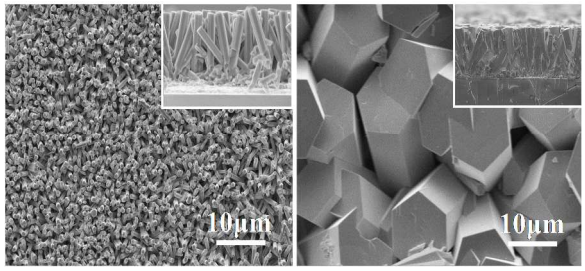

Fig. 7: SEM images of the films obtained from (a) fresh solution and (b) 30min aged solution for the 2nd stage deposition. The first stage deposition was kept unaltered at 30min (The inset shows the cross-section micrograph of the same films)

We studied the rinsing mechanism in detail to understand the need for the two-stage deposition. Rinsing with water, for example, can cause several changes that might activate the second state deposition process; (a) local change in pH, (b) (another) chemical heterogeneity in the solution, (c) temperature changes at the surface and (d) turbulence.

Rinsing with hot or cold water or even post rinsing heating of the substrate (at 60-70 ºC to dry it) has no visible effect in deposition rate. Also stirring the solution or simply shaking it never affected the second stage film growth. The above experiments show that neither temperature changes nor turbulence are likely to initiate the second stage growth.

To understand the effects of local change in pH and the chemical heterogeneity introduced by the rinsing step, we studied the rinsing step extensively by varying the chemical nature of the rinsing medium. There was no difference in film growth or structure if the substrate was rinsed after the first stage process with water (as was normally used) or with acid (both concentrated and dilute),which argues against a pH effect. If the substrate was rinsed with an aqueous solution of high pH (*e.g.*1 M NaOH solution), no deposition occurred during the second stage. However, since Mo oxides and oxide salts are soluble in alkaline solutions, this can be explained by dissolution of the Mo-

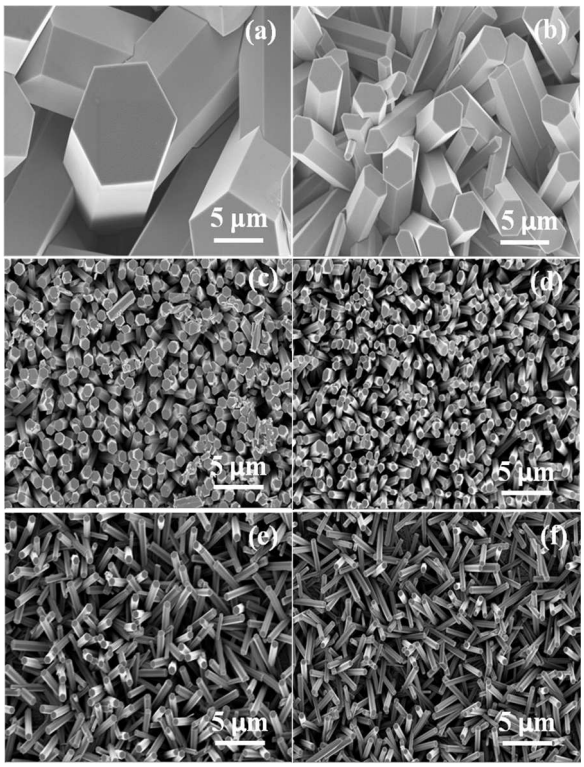

Fig. 8: SEM image of the films obtained from (a) 2 min, (b) 5 min, (c) 10 min (d) 20 min (e) 30 min and (f) 45 min of 1st stage deposition while the 2nd stage deposition was kept unaltered

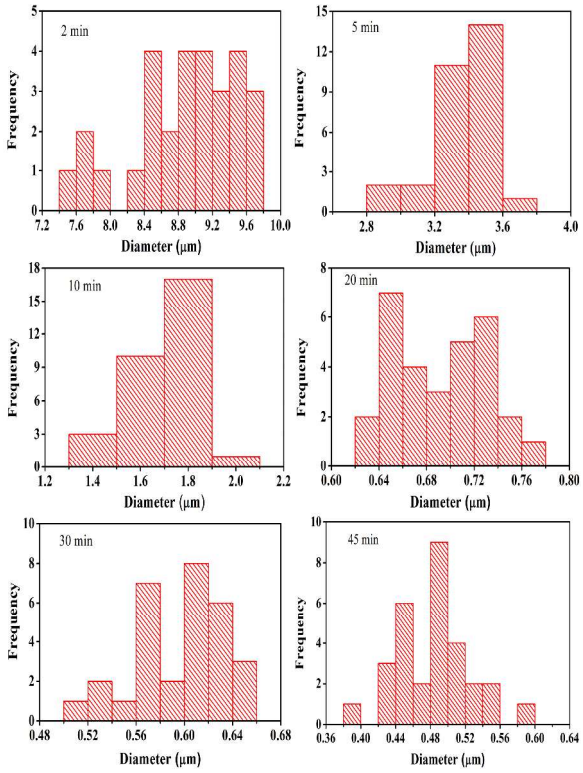

Fig. 9: Distribution of nanorod diameters of the films obtained from 2 min, 5 min, 10 min, 20 min, 30 min and 45 min of 1st stage deposition while the 2nd stage deposition was kept unaltered

O nuclei formed during the first stage and support the presence of such species after the first stage. However, if the substrate was rinsed with the same solution used in the first stage, there was no deposition in the second stage, regardless of the temperature of the rinsing solution. Therefore, the most likely cause of the rinsing after the first stage leading to deposition during the second stage is some chemical heterogeneity that provides the driving force for deposition in the second stage. Considering the well-known passivation of iron by strong HNO_3, a hypothesis is that rinsing the Mo-O nucleation layer removes a passivating film on the Mo-O which prevents continued growth during the first stage. However, since growth does occur after rinsing if the nucleated and rinsed substrate is re-immersed in the original solution, this hypothesis would require some difference between the Mo-O species formed in the first stage and that after rinsing with water that prevents the rinsed Mo-O species from being re-passivated. Regardless of the exact mechanism, it is clear that rinsing at the first stage changes the surface of the nucleation layer sufficiently for deposition to continue to occur.

Photocatalytic degradation of MB dye was observed in presence of *h*-MoO_3 nanorod films. Characteristic absorbance decreased with the time of light exposure as shown in the Figure 10. We believe that photogenerated charge carriers lead formation of hydroxyl or superoxide radicals that oxidized the MB molecules. The degradation of the MB dye can directly be observed by looking at its color that gets more transparent with time in the presence of h-MoO_3 film.

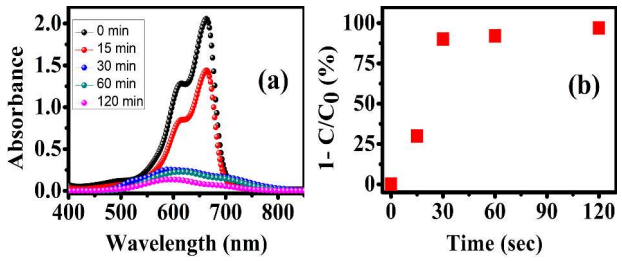

Fig. 10: (a) Absorbance plot of different MB solutions after different light exposure time in presence of h-MoO_3 nanorod films and (b) Plot of degradation percentage of MB with respect to light exposure time.

4. Conclusions

Thin films of highly crystalline hexagonal MoO_3 nanorods were deposited by chemical bath deposition. A two-step process where the samples were rinsed between the first and second step was necessary to achieve control over the growth and morphology of the films. Growth at the second stage was believed to be initiated by a chemical change of the nucleation centers formed in the first step caused by the rinsing step. Reasonable photocatalytic degradation of MB dye was observed using *h*-MoO_3 under visible light.

5. Acknowledgements

This work was supported partially by the National Center for Photovoltaics Research and Education (NCPRE) funded by the Ministry of New and Renewable Energy, Government of India.

Notes and References

[a] Department of Energy Science and Engineering,Indian Institute of Technology Bombay, Mumbai-400 076, India
[b] Department of Materials and Interfaces, Weizmann Institute of Science, Rehovot-76100, Israel

* Email: shaibal.sarkar@iitb.ac.in

1. J. Meyer, M. Kröger, S. Hamwi, F. Gnam, T. Riedl, W. Kowalsky and A. Kahn, *Appl. Phys. Lett.*, 2010, **96**, 193302.
2. C.-W. Chu, S.-H. Li, C.-W. Chen, V. Shrotriya and Y. Yang, *Appl. Phys. Lett.*, 2005, **87**, 193508.
3. H. Liu, M. Si, Y. Deng, A. T. Neal, Y. Du, S. Najmaei, P. M. Ajayan, J. Lou and P. D. Ye, *ACS Nano*, 2014, **8**, 1031.
4. J. Wang, K. C. Rose and C. M. Lieber, *J. Phys. Chem. B*, 1999, **103**, 8405.
5. Y. Bai, X. Liu, L. Chen, Khizar-ul-Haq, M. A. Khan, W. Q. Zhu, X. Y. Jiang and Z. L. Zhang, *Microelectron. J.*, 2007, **38**, 1185.
6. D. Qin, J. Liu, Y. Chen, C. Cheng and W. Quan, *Phys. status solidi A*, 2011, **208**, 1976.
7. M. Wang, Y. Li, H. Huang, E. D. Peterson, W. Nie, W. Zhou, W. Zeng, W. Huang, G. Fang, N. Sun, X. Zhao and D. L. Carroll, *Appl. Phys. Lett.*, 2011, **98**, 103305.
8. N. Li, B. E. Lassiter, R. R. Lunt, G. Wei and S. R. Forrest, *Appl. Phys. Lett.*, 2009, **94**, 023307.
9. I. Shakir, M. Shahid, H. W. Yang and D. J. Kang, *Electrochim. Acta*, 2010, **56**, 376.
10. R. Liang, H. Cao and D. Qian, *Chem. Commun.*, 2011, **47**, 10305.
11. L. Zhou, L. Yang, P. Yuan, J. Zou, Y. Wu and C. Yu, *J. Phys. Chem. C*, 2010, **114**, 21868.
12. P. Meduri, E. Clark, J. H. Kim, E. Dayalan, G. U. Sumanasekera and M. K. Sunkara, *Nano Lett.*, 2012, **12**, 1784.
13. S.-H. Lee, Y.-H. Kim, R. Deshpande, P. A. Parilla, E. Whitney, D. T. Gillaspie, K. M. Jones, A. H. Mahan, S. Zhang and A. C. Dillon, *Adv. Mater.*, 2008, **20**, 3627.
14. D. Y. Kim, J. Subbiah, G. Sarasqueta, F. So, H. Ding, Irfan and Y. Gao, *Appl. Phys. Lett.*, 2009, **95**, 093304.
15. C. Girotto, E. Voroshazi, D. Cheyns, P. Heremans and B. P. Rand, *ACS Appl. Mater. & Interfaces*, 2011, **3**, 3244.
16. A. Phuruangrat, D. J. Ham, S. Thongtem and J. S. Lee, *Electrochem. Comm.*, 2009, **11**, 1740.
17. H. Yang, X. Li, A. Wang, Y. Wang and Y. Chen, *Chin. J. Catal.*, 2014, **35**, 140.
18. Y. Chen, C. Lu, L. Xu, Y. Ma, W. Hou and J.-J. Zhu, *CrystEngComm*, 2010, **12**, 3740.
19. A. Chithambararaj, N. S. Sanjini, A. C. Bose and S. Velmathi, *Catal. Sci. Tech.*, 2013, **3**, 1405.
20. A. M. Taurino, A. Forleo, L. Francioso, P. Siciliano, M. Stalder and R. Nesper, *Appl. Phys. Lett.*, 2006, **88**, 152111.
21. T.-Y. Chang, Y.-W. Cheng and P.-T. Lee, *Appl. Phys. Lett.*, 2010, **96**, 043309.
22. X. W. Lou and H. C. Zeng, *Chem. Mater.*, 2002, **14**, 4781.
23. T. M. McEvoy, K. J. Stevenson, J. T. Hupp and X. Dang, *Langmuir*, 2003, **19**, 4316.
24. E. M. McCarron, *Chem. Commun.*, 1986, 336.
25. D. Z. Pai, K. K. Ostrikov, S. Kumar, D. A. Lacoste, I. Levchenko and C. O. Laux, *Sci. Rep.*, 2013, **3**, 1221 .

26. B. Baker, T. P. Feist and E. M. McCarron Iii, *J. Solid State Chem.*, 1995, **119**, 199.
27. V. Madhavi, P. Kondaiah, S. S. Rayudu, O. M. Hussain and S. Uthanna, *Mater. Express*, 2013, **3**, 135.
28. J. Zhou, N. S. Xu, S. Z. Deng, J. Chen, J. C. She and Z. L. Wang, *Adv. Mater.*, 2003, **15**, 1835.
29. I. Navas, R. Vinodkumar, K. J. Lethy, A. P. Detty, V. Ganesan, V. Sathe and V. P. M. Pillai, *J. Phys. D: Appl. Phys.*, 2009, **42**, 175305.
30. C. Liu, Z. Li and Z. Zhang, *Appl. Phys. Lett.*, 2011, **99**, 223104.
31. D. Parviz, M. Kazemeini, A. M. Rashidi and K. Jafari Jozani, *J. Nanopart. Res.*, 2010, **12**, 1509.
32. J. Song, X. Ni, D. Zhang and H. Zheng, *Solid State Sci.*, 2006, **8**, 1164.
33. N. Kumagai, N. Kumagai and K. Tanno, *Electrochim. Acta*, 1987, **32**, 1521.
34. H. J. Lunk, H. Hartl, M. A. Hartl, M. J. G. Fait, I. G. Shenderovich, M. Feist, T. A. Frisk, L. L. Daemen, D. Mauder, R. Eckelt and A. A. Gurinov, *Inorg. Chem.*, 2010, **49**, 9400.
35. Y. Xu, L. Xie, Y. Zhang and X. Cao, *Electr. Mater. Lett.*, 2013, **9**, 693.
36. A. Abdellaoui, L. Martin and A. Donnadieu, *Phys. Status Solidi A*, 1988, **109**, 455.
37. S. Deki, A. B. Béléké, Y. Kotani and M. Mizuhata, *J. Solid State Chem.*, 2009, **182**, 2362.
38. W. Pan, R. Tian, H. Jin, Y. Guo, L. Zhang, X. Wu, L. Zhang, Z. Han, G. Liu, J. Li, G. Rao, H. Wang and W. Chu, *Chem. Mater.*, 2010, **22**, 6202.
39. Z. Lei, X. Yang, J. Dong and X. Yi, *Chem. Mater.*, 2009, **21**, 5681.
40. V. V. Atuchin, T. A. Gavrilova, V. G. Kostrovsky, L. D. Pokrovsky and I. B. Troitskaia, *Inorg. Mater.*, 2008, **44**, 622.
41. G. R. .Patil, R. S. Gaikwad, M.B.Shelar, R. S. Mane, S. H. Hand and B. N. Pawar, *Arch. Phys. Res.*, 2012, **3**, 401.
42. M. Rouhani, Y. L. Foo, J. Hobley, J. Pan, G. S. Subramanian, X. Yu, A. Rusydi and S. Gorelik, *Appl. Surf. Sci.*, 2013, **273**, 150.
43. H. C. Cheng, C. F. Chen, C. Y. Tsay and J. P. Leu, *J. Alloy. Comp.*, 2009, **475**, L46.
44. L. L. Yang, Q. X. Zhao, M. Willander and J. H. Yang, *J. Crys. Growth*, 2009, **311**, 1046.
45. M. Kokotov and G. Hodes, *J. Mater. Chem.*, 2009, **19**, 3847.